Simulation of Fatigue Damage in Solder Joints using Cohesive Zones

Piet J.G. Schreurs, Müge Erinç, Adnan Abdul-Baqi, Marc G.D. Geers
Eindhoven University of Technology, Fac. Mech. Eng., Section of Materials Technology
Postbox 513, 5600 MB, Eindhoven, The Netherlands
p.j.g.schreurs@tue.nl

Abstract

Fatigue damage initiation and propagation in a solder bump, subjected to cyclic loading, is simulated using a cohesive zone methodology. Damage is assumed to occur at interfaces modeled through cohesive zones in the material, while the bulk material deforms elastoplastically. The state of damage at an interface is incorporated into the traction-displacement law of the cohesive zone by a damage variable. The gradual degradation of the interfaces and the corresponding damage accumulation throughout the cycling process is accounted for by an interfacial damage evolution law, which captures the main failure characteristics.

1 Introduction

Manufacturing in micro-electronics, especially for consumer applications, is driven by miniaturization for reasons of functionality enhancement and freedom of design. This is realised by integration of functionality into silicon, and also by packaging the silicon into miniature packages with high input/output ratio and power consumption. Lead-frame packages are therefore replaced by ball grid arrays (BGAs) where solder bumps connect chip and board both mechanically and electronically. Generally this miniaturization leads to elevated temperatures and high current densities. Differences in coefficient of thermal expansion (CTE) between printed circuit board (PCB), electronic component (chip package) and solder material, and also between the different phases in the solder alloy, lead to considerable thermomechanical loading. Due to repeated on-off switching of the device, cyclic loading results in the initiation and propagation of fatigue damage, which limits the lifetime and might be detrimental for the reliability of the components. The solder joints are susceptible to this thermomechanical damage.

Upto now the majority of solder joints is made from eutectic tin-lead alloy. The obvious toxicity of lead has made companies aware of the environmental effects and of the adverse public image of its applications. There are also several legislations on the use of lead in microelectronic components, mainly in Europe. A nearly complete ban of lead in consumer electronics is to be expected in the near future. A good replacement for the tin-lead alloy is a ternary eutectic alloy of tin (Sn), silver (Ag) and copper (Cu), generally referred to as SAC.

Due to the short design cycles of many electronic consumer devices, prototyping and testing is time consuming. Reliability of the electronic components must be assessed through numerical simulation during the design process. In reliability studies it is still common practice to model the solder joint as a continuous material with experimentally determined properties. To predict

the fatigue life of a solder joint, one loading cycle is simulated using the finite element method (FEM), and after calculating stresses and strains, the number of cycles to failure is determined according to a macroscopic fatigue life prediction model, eg. Coffin-Manson's law. There are, however, major drawbacks associated with this approach. The stresses and strains are calculated from a single loading cycle and the material properties of the solder are assumed to remain constant during the successive cycles. This assumption results in underestimated values of the fatigue life because in reality, repeated cycling results in a gradual degradation of the solder material [1]. Moreover, damage initiation sites, propagation paths and rates, remain unknown, which prohibits the (re)design of solder joint geometry and location. Finally, macroscopic fatigue limits are typically representative for homogeneous microstructures, and they do not account for the various sources of heterogeniety that are present in the solder joint, and which are generally not negligible with respect to the size of this connection.

Regarding the small dimensions of the solder joints, more realistic models should therefore account for the microstructure. It is well established that, during reflow, solder balls immediately react with the copper-pad or with the metallizations applied onto it. This generally leads to the formation of several intermetallic layers, with varying morphologies, at the solder/pad interface. Also due to the geometry of a solder bump, stress concentrations occur at these interfaces. The microstructural inhomogeneity and the stress concentrations in the material, contribute severely to the occurring fatigue damage. Experiments and common practice show that damage starts at and propagates along solder/pad interfaces in the material [2]. This interface damage can be modelled using a cohesive zone approach.

The cohesive zone method is a numerical tool to describe the mechanics of interfaces, that was initially developed to model crack initiation and growth in quasi-brittle materials. This method treats fracture as a gradual process in which separation between incipient material surfaces is resisted by cohesive tractions [3]. In comparison with fracture mechanics, the cohesive zone method has the advantages of smoothing the stress singularities at the crack tip and the easy adaptability to material and geometrical nonlinearities [4]. Compared to continuum damage mechanics, the cohesive zone method can be used to model cracking at interfaces between dissimilar materials. In the past decade, the method was mainly used to model cracking under monotonic loading conditions. The applicability to fatigue damage has quite recently started to receive attention [5, 6]. Damage, as a dissipative mechanism, can be accounted for explicitly, by incorporating a damage variable into the cohesive zone constitutive law, where the damage variable is supplemented by an evolution law to account for the accumulation of damage.

2 Cohesive zone model for interfacial fatigue damage

A cohesive zone is modelled as a four-noded element (Fig. 1) which may have zero initial thickness. Its constitutive behavior is specified through a relation between the relative opening displacement Δ_α and a corresponding traction T_α at the same location, with α being either the local normal (n) or tangential (t) direction in the cohesive zone mid-plane.

For the case of monotonic loading, the cohesive traction is characterized mainly by a peak value which represents the cohesive strength and a cohesive energy. An example of such tractions

are those given by Xu and Needleman [7]. Energy dissipation is accounted for by the softening branch in the curve as illustrated in Fig. 1, where δ_{n} and δ_{t} are characteristic lengths and $\sigma_{\max}$ and $\tau_{\max}$ are the peak tractions in the normal and tangential directions, respectively. Under monotonic loading, the cohesive traction reaches a peak value when a critical opening displacement is attained, then starts to diminish with the gradual increase of the opening displacement. This will result in the creation of two traction free surfaces, which marks the initiation of a crack or the extension of an existing one. Fracture characteristics of the material, such as fracture energy (the area under the traction curve) and fracture strength (the peak cohesive traction), are included in a typical cohesive zone constitutive relation [7]. Under cyclic loading, the situation is rather

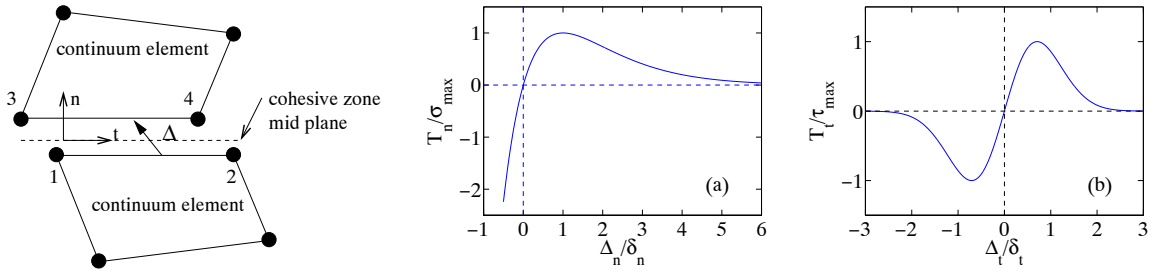

Figure 1: Cohesive zone illustration and monotonic normal and shear traction.

different. If the applied traction is less than the cohesive strength, the cohesive zone will have an infinite life. Fatigue experiments, however, indicate that under cyclic loading, materials fail at stress levels below their static fracture strength. Following the formulation of Chaboche et al. [4], we adopt a constitutive law in which the traction is a linear function of the separation, whereas the energy dissipation is accounted for by the incorporation of a nonlinear damage variable D_α into the constitutive law:

$$T_\alpha = k_\alpha(1 - D_\alpha)\Delta_\alpha \tag{1}$$

where k_α is the initial stiffness of the cohesive zone. D_α varies between zero (0) for damage-free cohesive zones and one (1) for completely damaged zones. The initial stiffness must be sufficiently high compared to the continuum stiffness such that, in the absence of damage, the cohesive zones artificial enhancement of the overall compliance is negligible. In this formulation, energy dissipation associated with the gradual degradation of the solder material is accounted for by the damage variable D_α only. An additional softening branch emerging from a nonlinear traction law would add an additional energy dissipation mechanism.

The damage variable is supplemented with an evolution law to account for the accumulation of damage throughout the cycling process. Motivated by the formulation of Roe and Siegmund [5], the following evolution law is here adopted:

$$\dot{D}_\alpha = c_\alpha |\dot{\Delta}_\alpha| \, (1 - D_\alpha + r)^{\mathrm{m}} \left\langle \frac{|T_\alpha|}{1 - D_\alpha} - \sigma_{\mathrm{f}} \right\rangle \tag{2}$$

where c_α is a constant, which controls the damage accumulation, $\dot{\Delta}_\alpha$ is the rate of the relative opening of the cohesive zone, r and m are constants which control the decay of the reaction force

at the final stage of damage and σ_{f} is the cohesive zone fatigue limit. Macauley brackets are used to prevent damage growth when the traction is below the endurance limit.

Incorporating the cohesive zones in the finite element formulation requires calculating the cohesive zone stiffness matrix and internal nodal force vector. The cohesive zone element is implemented as a "user element subroutine" in the MSC.Marc finite element package [8].

3 Solder joint model

Fig. 2 shows an ESEM[1] picture of a solder ball made of a SAC alloy (95.5Sn4.0Ag0.5Cu). In the bulk material distinct shades of gray indicate colonies, consisting of β-Sn dendrites in a matrix composed of a ternary eutectic phase mixture of (Sn), Ag_3Sn and Cu_6Sn_5. In a mounted arrangement the solder is applied between copper pads. In a detailed view of the SAC/copper-pad zone a thin layer of Cu_3Sn and a layer of Cu_6Sn_5 (≤ 5 μm) having scallop morphology can be observed. During reflow processes, depending on the cooling rate, occasional precipitation of primary Ag_3Sn occurs, nucleating at the Cu_6Sn_5 scallop tips and growing into the solder.

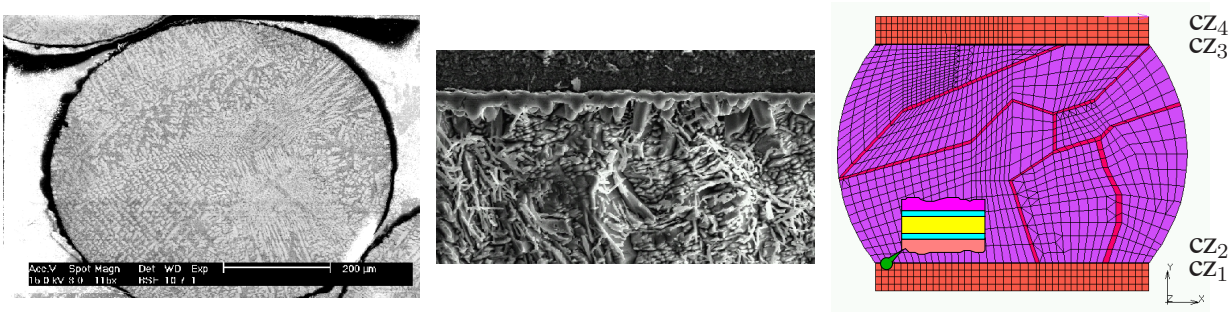

Figure 2: ESEM picture of SAC solder ball; interface zone (width = $\pm 50\mu$m); FEM model.

A single solder bump is modeled in plane strain, which is an approximation of the actual three-dimensional problem. The height of the bump is 1 mm as is the width of the pads. Cohesive zones with a thickness of $\pm 10\mu$m are located between colonies. The Cu_3Sn layer is not modeled, not only due to its small thickness but also because shear damage is not observed in this layer. The Cu_6Sn_5 layer has a thickness of 3 μm. Cohesive zones with a thickness of 0.1 μm are placed between this layer and the adjacent SAC and copper pad.

Material parameters

Indentation tests were used to measure the Young's modulus (E) of bulk material and intermetallics, according to the procedure described by Oliver and Pharr [9]. Tests were done with a MTS Nano-Indenter XP, equipped with a Berkovich indenter. Poisson's ratios (ν) of the components are taken from literature. With the Young's modulus known from direct measurement, the initial yield stress (σ_{v0}) and the linear hardening coefficient (H) of these materials could be determined with a hybrid approach, where the indentation tests were simulated with FEM and

[1] ESEM = Environmental Scanning Electronic Microscope

comparison of experimental and numerical load-indentation data provided the material parameters. The accuracy of this procedure was validated in separate investigations, were all material parameters of the test specimen were known in advance. The material parameters are listed in table 1.

			SAC	Cu	Cu_6Sn_5
Young's modulus	E	GPa	26.2	128.5	85.6
Poisson's ratio	ν	-	0.35	0.35	0.2
initial yield stress	σ_{v0}	MPa	22.0	175.0	100.0
hardening coefficient	H	GPa	0.83	4.15	3.70

Table 1: Material parameters for solder ball components.

Monotonous shear loading

A specimen consisting of three parallel copper plates, connected by SAC solder (Fig. 3) has been loaded with a computer controlled tensile stage. The solder is loaded in shear, where global shear strain increased monotonically to a maximum $\gamma_{max} = 8.9 \times 10^{-2}$ at a rate $\dot{\gamma} = 0.33 \times 10^{-2}$ s^{-1}.

As is shown in Fig. 3 void formation at the Cu/Cu_3Sn interface is observed as the primary damage mechanism under monotonic shear loading. Secondly, brittle cracking is seen in the Cu_6Sn_5 scallops with crack propagation in the direction of principle shear. Due to misalignment, bending caused delamination in some regions of the Cu_6Sn_5 scallops/solder interface.

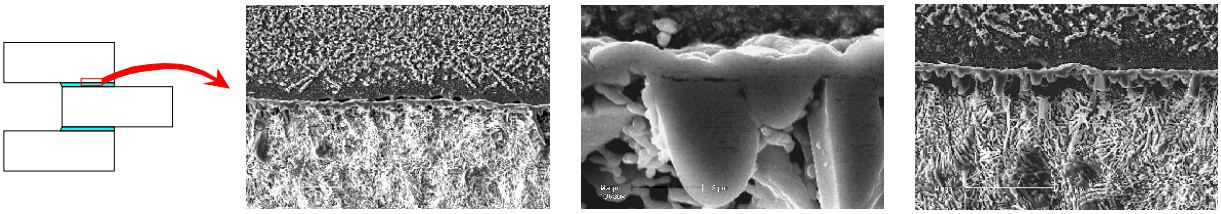

Figure 3: Shear specimen and interface cracks after monotonous shear loading.

It is expected that fatigue damage localizes at these physical interfaces and cohesive zones are thus embedded at these locations as was already described in Section 2. In tin-lead solder, damage has been reported at the trajectory along dendrite arm tips at the interface between colonies [10], so cohesive zones are also applied there.

Cohesive zones are assigned a high value for the initial stiffness $k_\alpha = 10^9$ MPa/mm, which is estimated by considering their initial thickness. For the current geometry (Fig. 2), this has been verified through the observation that using higher values for the initial stiffness has lead to identical reaction forces at the first cycle. Damage growth parameters for cyclic loading are not experimentally determined yet. Most non-ferrous alloys have no fatigue limit, so $\sigma_f = 0$ Pa. Parameter values for r and m are based on numerical analyses of simple tensile and shear tests. Also the values for c_n and c_t are extracted from numerical experiments. The distinction between different cohesive zones is made by assigning different values for these coefficients. Values are listed in table 2.

		c_n	c_t	r	m	σ_f
		mm/N	mm/N	-	-	Pa
Cu/Cu_3Sn	cz_1, cz_4	100	500	10^{-3}	3	0
Cu_6Sn_5/SAC	cz_2, cz_3	500	100	10^{-3}	3	0
colonies		150	150	10^{-3}	3	0

Table 2: Cohesive zone parameters for different interfaces.

Cyclic loading

Cyclic loading is applied by prescribing a sinusoidal x-displacement in the top-right node of the top boundary. The y-displacement of this node is alway suppressed. The y-displacement of all other points on the top boundary is either suppressed (TS) or free (TF). The prescribed sinusoidal x-displacement has an amplitude of 0.01 mm, which results in a maximum applied shear strain $\gamma_{\max} = 10^{-2}$. The lower boundary is fixed.

4 Solder joint fatigue damage

Fig. 4 shows the maximum deformation after 500 cycles for boundary conditions TS and TF, respectively. Displacements are scaled up 10 times to emphasize the deformation in the cohesive zones. Damage in the cohesive zones is also indicated with a color scale. The SAC/pad interfaces lose coherency almost completely. The normal and tangential damage in the cohesive zones at the lower pad is shown for $0 \leq x \leq 1$ mm for subsequent cycles. It is clearly seen that the tangential strength of cohesive zone 1 is reduced fast. The normal strength of zone 2 is reduced rapidly at the beginning and at the end of the zone where bending results in high normal stresses. For cohesive zones 3 and 4 at the upper pad, the same behaviour was observed, but is not shown here.

As damage progresses, the overall stiffness of the bump diminishes and the load required to attain the same strain level decreases. Fig. 5 shows the maximum and minimum values of the load during the subsequent cycles for the different boundary conditions. The discontinuous changes in the load for TS indicate the total loss of shear strength of the Cu/Cu_6Sn_5 interface zone at lower and upper pad, respectively.

An effective measure of the total damage in the solder bump is computed by averaging the local effective damage $D^{\mathrm{i}}_{\mathrm{eff}}$ over the entire bump :

$$D^{\mathrm{i}}_{\mathrm{eff}} = ({D^{\mathrm{i}}_{\mathrm{t}}}^2 + {D^{\mathrm{i}}_{\mathrm{n}}}^2 - D^{\mathrm{i}}_{\mathrm{t}} D^{\mathrm{i}}_{\mathrm{n}})^{1/2}. \qquad ; \qquad D_{\mathrm{eff}} = \frac{1}{A} \sum_{i=1}^{N_{\mathrm{cz}}} D^{\mathrm{i}}_{\mathrm{eff}} A^{\mathrm{i}}, \tag{3}$$

where A^{i} is the i^{th}cohesive zone area, A is the total area and N_{cz} is the number of cohesive zones. The evolution of the total effective damage throughout the cycling process is shown in Fig. 5. A rapid increase of damage at the initial cycling stage is followed by a much slower increase at the final stage. This can be explained by the fact that initially, when cohesive zones are undamaged, stresses and thus tractions are higher, resulting in a fast damage growth. The load transmitted through the damaged zones starts to decrease rapidly.

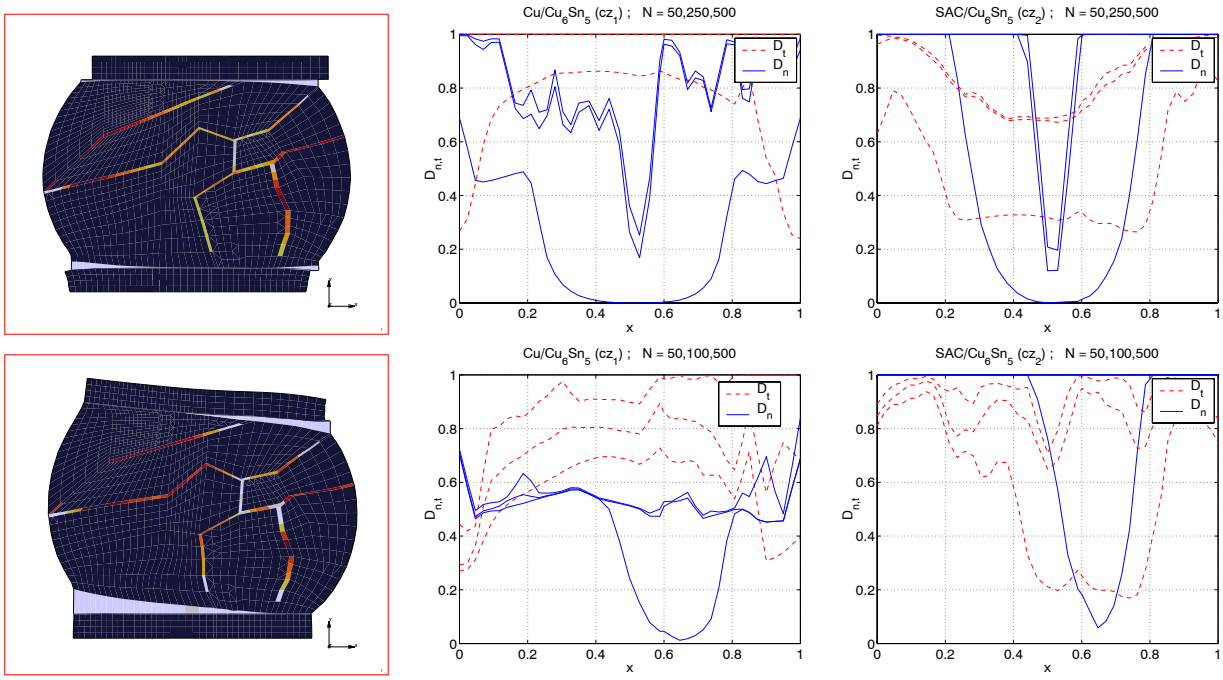

Figure 4: Left: bump deformation and damage in cohesive zones (low = dark, high = light). Right: damage along cohesive zones cz_1 and cz_2 at different cycles (N).

5 Concluding remarks

The cohesive zone approach seems promising in modeling fatigue damage in solder alloys. Gradual degradation of interfaces can be incorporated. Fatigue damage propagation paths emerge naturally during cyclic loading. The boundary conditions have a big influence, because they determine the loading of the cohesive zones.

In the near future the presented, rather simple traction-displacement law and damage evolution

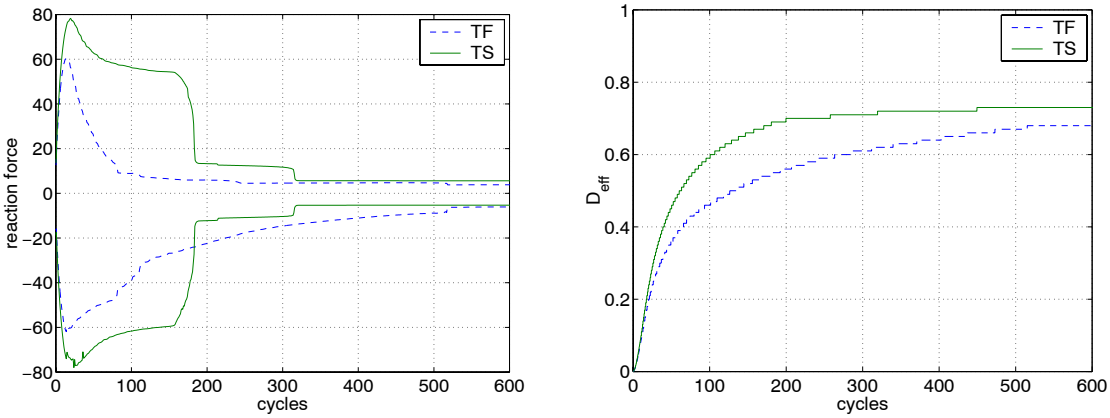

Figure 5: Load (left) and total effective damage (right) versus the number of cycles.

equation will be modified and enhanced such that simulated interfacial fatigue behavior in solder joints will be in accordance with detailed experimental observations. Cohesive zone parameters will be determined in an indirect manner. More realistic modeling of bulk material behaviour must incorporate time and temperature dependency. The detailed simulation of each individual cycle is time consuming. A major gain in the computational effort must be obtained by the use of a time homogenization technique.

References

[1] Basaran C., Tang H., Dishong T. and Searls D., *Advanced Packaging*, May 2001.

[2] Farooq M., Goldmann L., Martin G., Goldsmith C., Bergeron C., *Electronic Components and Technology Conference*, 2003

[3] Nguyen O., Repetto E.A., Ortiz M. and Radovitzky R.A., *International Journal of Fracture*, vol. **110**, 351–369, 2001.

[4] Chaboche J.L., Feyela F. and Monerie Y., *International Journal of Solids and Structures*, vol. **38**, 3127–3160, 2001.

[5] Roe K.L. and Siegmund T., *Engineering Fracture Mechanics*, vol. **70**, 209–232, 2003.

[6] Yang B., Mall S. and Ravi-Chandar K., *International Journal of Solids and Structures*, vol. **38**, 3927–3944, 2002.

[7] Xu X.-P. and Needleman A., *Model. Simul. Mater. Sci. Eng.*, vol. **1**, 111–132, 1993.

[8] MSC.Marc 2003, MSC.Software Corporation, 2003

[9] Oliver W.C., Pharr G.M., *J. of Materials Research*, vol. **7(6)**, 1564–1583, 1992.

[10] Matin M.A., Vellinga W.P. and Geers M.G.D., *Proceedings of the conference EuroSimE 2003*, Aix-en-Provence, 2003.